2014

A photoelectron spectroscopy and ab initio study of the structures and chemical bonding of the B_{25}^- cluster

Zachary A Piazza
Brown University

Ivan H. Popov
Utah State University

Wei-Li Li
Brown University

Rhitankar Pal
University of Nebraska-Lincoln

Xiao Cheng Zeng
University of Nebraska-Lincoln, xzeng1@unl.edu

See next page for additional authors

A photoelectron spectroscopy and *ab initio* study of the structures and chemical bonding of the B_{25}^- cluster

Zachary A. Piazza,[1,a)] Ivan A. Popov,[2,a)] Wei-Li Li,[1] Rhitankar Pal,[3] Xiao Cheng Zeng,[3] Alexander I. Boldyrev,[2,b)] and Lai-Sheng Wang[1,b)]
[1]*Department of Chemistry, Brown University, Providence, Rhode Island 02912, USA*
[2]*Department of Chemistry & Biochemistry, Utah State University, Logan, Utah 84322, USA*
[3]*Department of Chemistry, University of Nebraska-Lincoln, Lincoln, Nebraska 68588, USA*

(Received 25 March 2014; accepted 9 May 2014; published online 17 July 2014)

Photoelectron spectroscopy and *ab initio* calculations are used to investigate the structures and chemical bonding of the B_{25}^- cluster. Global minimum searches reveal a dense potential energy landscape with 13 quasi-planar structures within 10 kcal/mol at the CCSD(T)/6-311+G(d) level of theory. Three quasi-planar isomers (**I**, **II**, and **III**) are lowest in energy and nearly degenerate at the CCSD(T) level of theory, with **II** and **III** being 0.8 and 0.9 kcal/mol higher, respectively, whereas at two density functional levels of theory isomer **III** is the lowest in energy (8.4 kcal/mol more stable than **I** at PBE0/6-311+G(2df) level). Comparison with experimental photoelectron spectroscopic data shows isomer **II** to be the major contributor while isomers **I** and **III** cannot be ruled out as minor contributors to the observed spectrum. Theoretical analyses reveal similar chemical bonding in **I** and **II**, both involving peripheral 2c-2e B−B σ-bonding and delocalized interior σ- and π-bonding. Isomer **III** has an interesting elongated ribbon-like structure with a π-bonding pattern analogous to those of dibenzopentalene. The high density of low-lying isomers indicates the complexity of the medium-sized boron clusters; the method dependency of predicting relative energies of the low-lying structures for B_{25}^- suggests the importance of comparison with experiment in determining the global minima of boron clusters at this size range. The appearance of many low-lying quasi-planar structures containing a hexagonal hole in B_{25}^- suggests the importance of this structural feature in maintaining planarity of larger boron clusters.
 [http://dx.doi.org/10.1063/1.4879551]

I. INTRODUCTION

Boron is an electron-deficient element with a capacity to form strong covalent bonds with other elements. Boron-containing systems have been investigated extensively in hopes of discovering nanomaterials with novel structures and properties. While extended boron-nitride sheets have been produced and shown to be atom-thin nano-insulators,[1–4] pure boron nanostructures have been studied primarily through theoretical and computational means. The structures and bonding of size-selected negatively charged boron clusters (B_n^-) have been systematically investigated up to $n = 24$ through joint experimental and theoretical studies,[5–19] as well as subsequent computational works.[20–22] Interestingly, the anionic boron clusters are found to remain planar or quasi-planar in this size range. Cationic boron clusters (B_n^+) have been observed experimentally and investigated through ion mobility measurements combined with theoretical calculations in the small size range.[23–27] Some boron clusters were shown to undergo unprecedented internal rotations, a phenomenon that led to the suggestion of molecular Wankel motors,[20,25,26] inspired by the doubly concentric spider-web-like structure of B_{19}^-.[14] One more quasi-planar member of the so-called "Wankel motor" family, B_{18}^{2-}, was recently found.[22] Neutral boron clusters have been challenging to study experimentally and they have been found computationally to be three-dimensional (3D) at B_{20}, for which a double-ring structure was found to be more stable than two-dimensional (2D) structures.[11] This conclusion has been reinforced by more recent calculations.[28] However, the 3D double-ring global minimum found computationally was not detected in a recent infrared experiment.[29] Large fullerene-like cage structures of boron clusters have also been investigated theoretically. A B_{80} fullerene structure with icosahedral symmetry was proposed,[30] although subsequent calculations demonstrate that a number of low-symmetry 3D structures involving stuffed cages are more stable.[31–36] Constrained global minimum searches reveal a rugged potential energy surface, where many similar low-energy and low-symmetry structures exist.

Concurrent to our joint experimental and theoretical investigations of the structures and bonding of size-selected boron clusters, there have been increasing interests about extended 2D boron sheets and boron nanotubes.[37–48] Extended boron sheets consisting of a triangular lattice were found to be buckled.[37] Highly stable and truly planar 2D boron sheets were found computationally by removing boron atoms from the triangular lattice to create hexagonal holes.[38,39] It was found that a ratio of one hexagonal hole to every eight boron atoms optimal, which was called a α-sheet.[38] The electronic properties of the α-sheet were further investigated through

[a)]Z. A. Piazza and I. A. Popov contributed equally to this work.
[b)]Authors to whom correspondence should be addressed. Electronic addresses: a.i.boldyrev@usu.edu and lai-sheng_wang@brown.edu

orbital localization, which suggests that the hexagonal holes enhance the stability of the α-sheet by reducing unfavorable electron-electron repulsion through π-electron delocalization over the hole region.[44] Even though there have been computational studies of possible syntheses of the α-sheet on suitable substrates,[47,48] experimental realization of this novel nanostructure is expected to be challenging. However, the viability of extended boron sheets with hexagonal holes was corroborated in a recent photoelectron spectroscopy (PES) and theoretical study of the B_{36}^- and B_{36} clusters.[49] The B_{36} cluster is found to be quasi-planar with hexagonal symmetry and a perfect central hexagonal hole. The hexagonal B_{36} cluster can be viewed as a potential basis for the extended boron sheet, providing the first experimental evidence that the 2D atom-thin boron layer with hexagonal holes is viable. A name "borophene" was coined to designate the putative 2D atom-thin boron sheets in analogy to graphene.[49] Tetragonal and pentagonal holes have been observed in smaller boron clusters, but the B_{36}^- and B_{36} clusters represent the first boron clusters to feature an interior hexagonal hole. Very recently, an inherently chiral boron cluster, B_{30}^-, with a hexagonal vacancy has been reported,[50] even though neutral B_{30} appears to have a very different potential energy surface.[51] It is expected that hexagonal holes will be a defining feature for large planar boron clusters.

With the increasing current interest in boron-based nanostructures, systematic investigations of size-selected boron clusters remain an important avenue for discovery. Herein, we report a joint PES and theoretical study of the B_{25}^- cluster. Extensive effort was carried out to search for the low-lying structures of B_{25}^- using three methods: Coalescence Kick (CK),[15] Cartesian Walking (CW),[16] and Basin Hopping (BH).[52] Thirteen quasi-planar structures are found to be within 10 kcal/mol relative to the lowest energy structure calculated at the coupled-cluster level of theory. Such a high density of low-lying isomers is unprecedented in anionic boron clusters that we have studied thus far. Two quasi-planar structures (**I** and **II**) both with 15 peripheral atoms and 10 inner atoms are found to be nearly degenerate at the coupled-cluster level of theory. The simulated spectrum of isomer **II** with a pentagonal hole is shown to agree well with the observed PES spectrum, whereas isomer **I** with a tetragonal and a pentagonal hole cannot be completely ruled out and may also be populated as a minor species in the experiment. A third quasi-planar isomer (**III**) is characterized by a ribbon-like buckled structure and can be viewed as extensions to the ribbon-like global minima of B_{13}^- and B_{16}^-.[9,12] The simulated spectrum of isomer **III** displays certain resemblance to the experimental spectrum, suggesting that this isomer could also be present in the cluster beam.

II. EXPERIMENTAL AND COMPUTATIONAL METHODS

A. Photoelectron spectroscopy

The experiment was carried out using a magnetic-bottle PES apparatus equipped with a laser vaporization cluster source, details of which can be found elsewhere.[53] Briefly, negatively charged boron clusters were produced by laser vaporization of a hot-pressed ^{10}B isotopically enriched (96%) disk target. The clusters were entrained in a He carrier gas containing 5% Ar and underwent a supersonic expansion to form a collimated and cold cluster beam. The cluster cooling was controlled by the resident time of the clusters in the nozzle and the supersonic expansion.[54,55] Negatively charged clusters were extracted from the cluster beam and analyzed with a time-of-flight mass spectrometer. The B_{25}^- cluster of current interest was mass-selected and decelerated before being intercepted by a detachment laser beam. For the current study, the 193 nm (6.424 eV) radiation from an ArF excimer laser was used. Photoelectrons were collected at nearly 100% efficiency by a magnetic bottle and analyzed in a 3.5 m long electron flight tube. The spectrum was calibrated using the known spectra of Bi^- and the electron energy resolution of the apparatus was $\Delta E_k/E_k \sim 2.5\%$, i.e., ~25 meV for 1 eV electrons.

B. Global minimum searches and computational methods

We searched for the global minimum and low lying isomers of B_{25}^- using three methods: the CK method,[15] the CW method,[16] and the BH method.[52] In brief, the CK method creates a population of trial structures by randomly generating coordinates in a box,[56] then gradually pushes the atoms towards the molecular center of mass to eliminate fragmented cluster structures from the population. Once this coalescence procedure is complete, trial structures are further optimized to their closest minima. These calculations are conducted using the DFT formalism for energy evaluations. The CW method also considers a large population of structures which are optimized using DFT. In CW, trial structures are generated by placing an atom down at each step of a constrained random-walk upon a grid of Cartesian coordinate points. In the current work, we used primarily 2D grids to bias the CW population towards planar and quasi-planar structures. Both the CK and CW searches were conducted using the PBE0 exchange correlation functional[57] and the 3-21G basis set,[58] while the BH searches used the PBE exchange correlation functional[59] with the DND basis set.[60] Approximately 10 000 structures were evaluated using CK, roughly 3000 were evaluated using CW, and roughly 250 structures with BH. We also investigated a double-ring structure for B_{25}^- that was built manually, because low-energy double-ring structures are known to be present for several other anionic boron clusters.[11,17,18] However, the double-ring structures have not been observed experimentally for any neutral or anionic boron clusters.[29]

Following the global minimum searches, we refined the structures of the low-lying isomers using two DFT functionals, PBE0[57] and TPSSh,[61] and the more expansive 6-311+G(d) basis set.[62,63] Single-point energy calculations were further performed at four different levels of theory to give as accurate relative energies as possible: PBE0/6-311+G(2df)//PBE0/6-311 +G(d), TPSSh/6-311+G(2df)//TPSSh/6-311+G(d), CCSD/6-311+G(d)//PBE0/6-311 +G(d),[63,64] and CCSD(T)/6-311+G(d)//PBE0/6-311

+G(d).[65,66] Frequency analyses at DFT/6-311+G(d) were conducted to ensure that each structure is a minimum on the potential energy surface. Zero-point energy (ZPE) corrections were made to the energies at the corresponding level of theory for each DFT method, while the ZPE corrections for the CCSD and CCSD(T) energies were done using the corresponding PBE0 values.

For comparison with the experimental PES data, we calculated vertical detachment energies (VDEs) for all isomers with a relative energy under 10 kcal/mol at the CCSD(T)/6-311+G(d)/PBE0/6-311+G(d) level. The VDE calculations were done at two levels of theory: the outer valence Green's function method[67–69] (ROVGF/6-311+G(2df)//PBE0/6-311+G(d)) and the time-dependent DFT method[70,71] (TD-PBE0/6-311+G(2df)//PBE0/6-311+G(d)). In the ROVGF method, VDEs were calculated through the corrections to the orbital energies due to electron correlation and electron relaxation. We used the frozen core approximation in treating the electron correlation and a partial transformation approach with the OVGF window set up to the last ten molecular orbitals. With the TD-PBE0 method, the first VDE was calculated as the energy difference between the ground electronic state of the anion and the lowest doublet electronic state of the neutral at the geometry of the anion and at the respective levels of theory. Vertical excitation energies from the neutral states were then calculated and added to the first VDE to approximate the higher VDEs.

Chemical bonding analyses were performed for the two lowest-lying isomers using the adaptive natural density partitioning (AdNDP) method,[72] which has been used successfully for bare and doped boron clusters,[19,73–75] as well as 2D nanostructures of boron and carbon.[76,77] The AdNDP method analyzes the first-order reduced density matrix to obtain local block eigenfunctions with optimal convergence properties for an electron density description. The obtained local blocks correspond to the sets of *n*-atoms (*n* ranging from one to the total number of atoms in the molecule) that are tested for the presence of *n*-electron objects [*n*-center two electron (*n*c-2e) bonds], including core electrons and lone pairs as a special case of $n = 1$. The user-directed form of the AdNDP analysis can be applied to specified molecular fragments and is analogous to the directed search option of the standard natural bond orbital (NBO) method.[78,79] AdNDP accepts only those bonding elements whose occupation numbers (ONs) exceed specified threshold values which are usually chosen to be close to 2.0 |e|. The AdNDP method recovers both Lewis bonding elements (1c-2e and 2c-2e objects) and delocalized bonding elements associated with the concepts of aromaticity and antiaromaticity. Hence, AdNDP achieves a seamless description of systems featuring both localized and delocalized bonding. The AdNDP analyses were done at the B3LYP/6-31G level.

All DFT calculations with the PBE0 and TPSSh functionals, CCSD, CCSD(T), TD-DFT, and OVGF calculations were performed with the GAUSSIAN 09 program.[80] PBE calculations with the DNP basis set were carried out using the Dmol3 program.[60] Structural and molecular orbital (MO) visualizations were performed using GaussView 3.0[80] and MOLEKEL 5.4.0.8.[81]

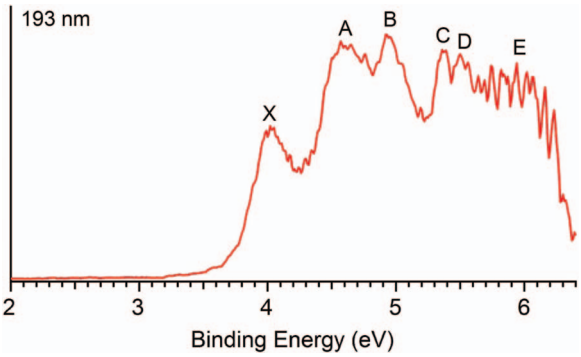

FIG. 1. Photoelectron spectrum of B_{25}^- at 193 nm.

III. EXPERIMENTAL RESULTS

The photoelectron spectrum of B_{25}^- at 193 nm is shown in Fig. 1. The detachment features are labeled with letters denoting the observed PES bands, which should correspond to detachment transitions to the neutral ground state (X) and neutral excited states (A, B, ...). The band maximum corresponds to the VDE of each detachment transition. However, for complex systems with a high density of electronic states, individual detachment transitions may not be resolved. In such cases, the observed VDE represents the average of several detachment channels. The measured VDEs for B_{25}^- are summarized in Table I, where they are compared with the theoretical data.

The B_{25}^- spectrum exhibits three relatively broad spectral bands in the low binding energy region and congested features in the high binding energy region above 5.2 eV. The X band yielded a VDE of 4.02 ± 0.06 eV for the detachment transition to the neutral ground state. The adiabatic detachment energy (ADE) of the ground state transition is estimated to be 3.8 ± 0.1 eV from the leading edge of the X band. The ADE also presents the electron affinity of the corresponding neutral B_{25}. The large uncertainty is assessed because of the tail on the low binding energy side, which can be due to a combination of factors, i.e., hot bands and isomeric contributions of the anion or large geometry changes between the anionic and neutral ground state. Following an energy gap of ~0.5 eV, two broad features A (4.6 ± 0.1 eV) and B (4.94 ± 0.06 eV) are observed, each of which may contain more than one detachment channel, in particular, for band A. At the high binding energy side, we observe two partially resolved bands C (5.37 ± 0.05 eV) and D (5.50 ± 0.05 eV). Beyond band D, continuous signals are observed, which are designated as E (~6.0) for the sake of discussion.

IV. COMPUTATIONAL RESULTS

Our global minimum searches revealed 51 isomers within 35 kcal/mol at the PBE0/6-311+G(d) level of theory. The 30 lowest isomers along with their relative energies at all four levels of theory can be found in the supplementary material (Fig. S1).[82] Single-point energies were calculated at the CCSD(T)/6-311+G(d) level of theory using the optimized PBE0/6-311+G(d) geometries for the 20 lowest isomers. An abbreviated, set of these isomers is presented in

TABLE I. The observed vertical detachment energies (VDEs) for B_{25}^- and comparison with calculated VDEs for isomers **I** (C_1, ^1A), **II** (C_1, ^1A), and **III** (C_{2v}, $^1A_1$) at two levels of theory. All energies are in eV.

Feature	VDE (Expt.)[a]	Final state and electronic configuration	VDE (theor.) TD-PBE0[b]	VDE (theor.) ROVGF[c]
		Isomer II (C_1, ^1A)		
X[d]	4.02(6)	$^2A\ldots(30a)^2(31a)^2(32a)^2(33a)^2(34a)^2(35a)^2(36a)^2(37a)^2(38a)^1$	3.97	4.01
A	4.6(1)	$^2A\ldots(30a)^2(31a)^2(32a)^2(33a)^2(34a)^2(35a)^2(36a)^2(37a)^1(38a)^2$	4.51	4.53
		$^2A\ldots(30a)^2(31a)^2(32a)^2(33a)^2(34a)^2(35a)^2(36a)^1(37a)^2(38a)^2$	4.70	4.76
B	4.94(6)	$^2A\ldots(30a)^2(31a)^2(32a)^2(33a)^2(34a)^2(35a)^1(36a)^2(37a)^2(38a)^2$	4.93	4.52
C	5.37(5)	$^2A\ldots(30a)^2(31a)^2(32a)^2(33a)^2(34a)^1(35a)^2(36a)^2(37a)^2(38a)^2$	5.35	5.47
D	5.50(5)	$^2A\ldots(30a)^2(31a)^2(32a)^2(33a)^1(34a)^2(35a)^2(36a)^2(37a)^2(38a)^2$	5.65	5.64
E	∼6.0	$^2A\ldots(30a)^2(31a)^2(32a)^1(33a)^2(34a)^2(35a)^2(36a)^2(37a)^2(38a)^2$	6.06	6.03
		$^2A\ldots(30a)^2(31a)^1(32a)^2(33a)^2(34a)^2(35a)^2(36a)^2(37a)^2(38a)^2$	6.15	[e]
		$^2A\ldots(30a)^1(31a)^2(32a)^2(33a)^2(34a)^2(35a)^2(36a)^2(37a)^2(38a)^2$	6.95	[e]
		Isomer III (C_{2v}, $^1A_1$)		
		$^2B_1\ldots(9b_2)^2(11a_1)^2(7b_1)^2(10b_2)^2(8b_1)^2(6a_2)^2(12a_1)^2(7a_2)^2(9b_1)^1$	4.11	3.89
		$^2A_2\ldots(9b_2)^2(11a_1)^2(7b_1)^2(10b_2)^2(8b_1)^2(6a_2)^2(12a_1)^2(7a_2)^1(9b_1)^2$	4.58	4.40
		$^2A_1\ldots(9b_2)^2(11a_1)^2(7b_1)^2(10b_2)^2(8b_1)^2(6a_2)^2(12a_1)^1(7a_2)^2(9b_1)^2$	4.91	4.91
		$^2A_2\ldots(9b_2)^2(11a_1)^2(7b_1)^2(10b_2)^2(8b_1)^2(6a_2)^1(12a_1)^2(7a_2)^2(9b_1)^2$	5.01	5.02
		$^2B_1\ldots(9b_2)^2(11a_1)^2(7b_1)^2(10b_2)^2(8b_1)^1(6a_2)^2(12a_1)^2(7a_2)^2(9b_1)^2$	5.54	5.50
		$^2B_2\ldots(9b_2)^2(11a_1)^2(7b_1)^2(10b_2)^1(8b_1)^2(6a_2)^2(12a_1)^2(7a_2)^2(9b_1)^2$	6.03	6.13
		$^2B_1\ldots(9b_2)^2(11a_1)^2(7b_1)^1(10b_2)^2(8b_1)^2(6a_2)^2(12a_1)^2(7a_2)^2(9b_1)^2$	6.04	6.20
		$^2A_1\ldots(9b_2)^2(11a_1)^1(7b_1)^2(10b_2)^2(8b_1)^2(6a_2)^2(12a_1)^2(7a_2)^2(9b_1)^2$	6.33	6.55
		Isomer I (C_1, ^1A)		
		$^2A\ldots(30a)^2(31a)^2(32a)^2(33a)^2(34a)^2(35a)^2(36a)^2(37a)^2(38a)^1$	4.29	4.39
		$^2A\ldots(30a)^2(31a)^2(32a)^2(33a)^2(34a)^2(35a)^2(36a)^2(37a)^1(38a)^2$	4.56	4.56
		$^2A\ldots(30a)^2(31a)^2(32a)^2(33a)^2(34a)^2(35a)^2(36a)^1(37a)^2(38a)^2$	4.93	4.77
		$^2A\ldots(30a)^2(31a)^2(32a)^2(33a)^2(34a)^2(35a)^1(36a)^2(37a)^2(38a)^2$	4.94	4.90
		$^2A\ldots(30a)^2(31a)^2(32a)^2(33a)^2(34a)^1(35a)^2(36a)^2(37a)^2(38a)^2$	5.20	5.17
		$^2A\ldots(30a)^2(31a)^2(32a)^2(33a)^1(34a)^2(35a)^2(36a)^2(37a)^2(38a)^2$	5.64	5.80
		$^2A\ldots(30a)^2(31a)^2(32a)^1(33a)^2(34a)^2(35a)^2(36a)^2(37a)^2(38a)^2$	6.01	5.86
		$^2A\ldots(30a)^2(31a)^1(32a)^2(33a)^2(34a)^2(35a)^2(36a)^2(37a)^2(38a)^2$	6.46	6.46

[a]Numbers in the parentheses represent uncertainties in the last digit.
[b]VDEs were calculated at the TD-PBE0/6-311+G(2df)//PBE0/6-311+G(d) level of theory.
[c]VDEs were calculated at the ROVGF/6-311+G(2df)//PBE0/6-311+G(d) level of theory.
[d]Adiabatic detachment energy (ADE) of B_{25}^- is estimated to be 3.8 ± 0.1 eV.
[e]A value was not able to be calculated at this level of theory.

Fig. 2. The simulated spectra of all isomers under 10 kcal/mol at the CCSD(T)/6-311+G(d)//PBE0/6-311+G(d) level of theory are given in the supplementary material as Table S1.[82] The Cartesian coordinates of the first 30 isomers at PBE0/6-311+G(d) are given in Table S2 in the supplementary material.

We found three nearly degenerate, quasi-planar structures, competing for the global minimum. According to the highest level of theory we employed, CCSD(T)/6-311+G(d), the three structures are separated by 0.9 kcal/mol (Fig. 2). Figure 3 compares the relative energies of these three structures, labeled as **I**, **II**, and **III** at four levels of theory. We find that the relative ordering of isomers **I**, **II**, and **III** is dependent on the theoretical methods employed. Both DFT methods, PBE0/6-311+G(2df)//PBE0/6-311+G(d) and TPSSh/6-311+G(2df)//TPSSh/6-311+G(d), and CCSD/6-311+G(d)//PBE0/6-311+G(d) predict isomer **III** is lowest in energy, while the highest level of theory employed, CCSD(T)/6-311+G(d)//PBE0/6-311+G(d), predicts isomer **I** to be lowest in energy. Clearly, the current levels of theory are not able to distinguish which one is the true global minimum. Multiple isomers competing for the global minimum are not unprecedented for boron clusters. We have found previously that the closed-shell B_{21}^- cluster exhibits two close-lying isomers, with similar geometric and electronic properties, within 2 kcal/mol at the CCSD(T)/6-311+G(d) level of theory.[16] For the open shell B_{22}^- cluster, we found two lowest quasi-planar isomers within 1.0 kcal/mol at the CCSD(T)/6-311+G(d) level.[17]

Structures **I** and **II** of B_{25}^- possess similar geometric characteristics and both can be considered as quasi-planar derivatives of the familiar triangular boron lattice with out-of-plane buckling. Both have 15 peripheral atoms and 10 inner atoms and a pentagonal hole. The most notable differences are that isomer **I** has a pentagonal hole and a tetragonal hole, both on the edge, while isomer **II** has only a pentagonal hole in the interior of the cluster. Isomer **I** is directly related to the global minimum of B_{24}^-,[18] simply by adding one boron atom to the interior region of the cluster (see Fig. S2).[82] While the deviation from planarity in B_{24}^- is somewhat localized with a maximum out-of-plane distortion of ∼1.2 Å, isomer **I** of B_{25}^- deviates from planarity by ∼1.8 Å. The interior

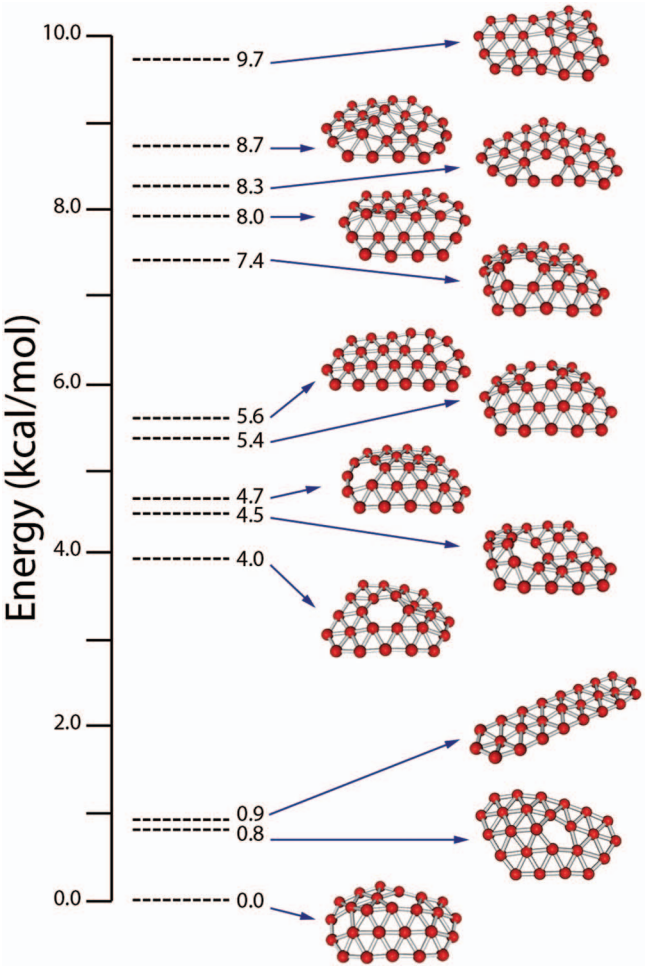

FIG. 2. Relative energies in kcal/mol of the lowest lying isomers of B_{25}^- obtained from global minimum searches based on the CCSD(T)/6-311+G(d)//PBE0/6-311+G(d) method. Sticks drawn between atoms represent interatomic distances <2.0 Å; they do not necessarily represent single B–B σ bonds here and elsewhere.

pentagonal hole of isomer **II** is reminiscent of the global minimum of neutral B_{30}.[50,51] Isomer **III** has a distinct ribbon-like geometry, characterized by an elongated three-row buckled triangular lattice reminiscent of the global minima previously reported for B_{13}^- and B_{16}^-.[9,12] As discussed in detail later, the simulated spectrum of isomer **II** is in very good agreement with the experiment, while isomers **I** and **III** cannot be ruled out as contributing to the experimental features.

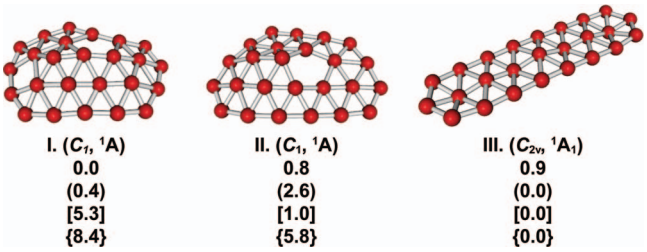

FIG. 3. The ground electronic states and relative energies of the three lowest lying isomers of B_{25}^-. Energies are given at CCSD(T)/6-311+G(d)//PBE0/6-311+G(d), CCSD/6-311+G(d)//PBE0/6-311+G(d) (in parenthesis), PBE0/6-311+G(2df)//PBE0/6-311+G(d) (in square brackets), and TPSSh/6-311+G(2df)//TPSSh/6-311+G(d) (in curly brackets) in kcal/mol. The CCSD(T) and CCSD values are corrected for zero-point energies at the PBE0/6-311+G(d) level of theory, while the PBE0 and TPSSh values are corrected using the corresponding DFT/6-311+G(d) zero-point energies.

A 3 kcal/mol gap separates isomers **I**-**III** from a dense manifold of higher-lying isomers (Fig. 2). Isomer **IV** lies at 4.0 kcal/mol relative to isomer **I**, and consists of 15 peripheral atoms and 10 inner atoms similar to **I** and **II**. This isomer contains a distinct hexagonal hole akin to that seen in the hexagonally symmetric global minima of B_{36}^- and B_{36}.[49] More structures with hexagonal holes of various degrees of distortions are observed at 4.5, 4.7, 5.4, and 7.4 kcal/mol above the global minimum (Fig. 2). A total of seven structures containing a hexagonal hole are found within 15 kcal/mol at the CCSD(T)/6-311+G(d) level of theory (Fig. S1).[82]

V. COMPARISON BETWEEN THEORY AND EXPERIMENT

All the low-lying isomers of B_{25}^- are closed shell, and thus only doublet neutral states result upon single electron detachment. The calculated VDEs and simulated photoelectron spectra of all isomers below 10 kcal/mol at the CCSD(T) level of theory are presented in Table S1.[82] We find that the calculated VDEs of isomer **II** show excellent agreement with the experiment at both the TD-PBE0 and ROVGF levels of theory, while isomers **I** and **III** also display certain features consistent with the observed spectrum and may be present experimentally. Thus, our discussion will only focus on isomers **I**-**III**. The calculated VDEs at the TD-PBE0 and ROVGF levels of theory for isomers **I**-**III** are presented in Table I along with the experimental VDEs. Simulated spectra of isomers **I**-**III**, obtained by fitting a Gaussian function with 0.1 eV FWHM (full width at half maximum) to each VDE, are compared with the experimental spectrum in Fig. 4. As shown in Table I, both TD-PBE0 and ROVGF methods predict similar VDEs. We will primarily use the TD-PBE0 values in the following discussion.

A. Isomer II

The TD-PBE0 method predicts the first VDE for B_{25}^- as 3.97 eV, resulting from removal of an electron from the doubly occupied HOMO of isomer **II**, in excellent agreement with the measured VDE of the X band at 4.02 eV (Table I). Following an energy gap, the second and third VDEs are calculated to be 4.51 and 4.70 eV, corresponding to electron detachment from the HOMO−1 and HOMO−2 of isomer **II**, respectively. These two VDEs are fairly close to each other, agreeing well with the broadband A at 4.6 eV. The fourth VDE is predicted to be 4.93 eV, in excellent agreement with band B at 4.94 eV. Following another energy gap, a set of four closely spaced detachment channels with VDEs in the range of 5.35–6.16 eV are predicted, consistent with the congested PES features observed in the high binding energy side (Figs. 1 and 4). The one major discrepancy between TD-PBE0 and ROVGF occurs around the range of the experimental peak B with the VDE of 4.94 eV. While TD-PBE0 predicts a VDE of 4.93 eV from electron detachment from HOMO−3 (in excellent agreement with peak B), the corresponding ROVGF value lies at 4.52 eV (Table I). The two methods give almost

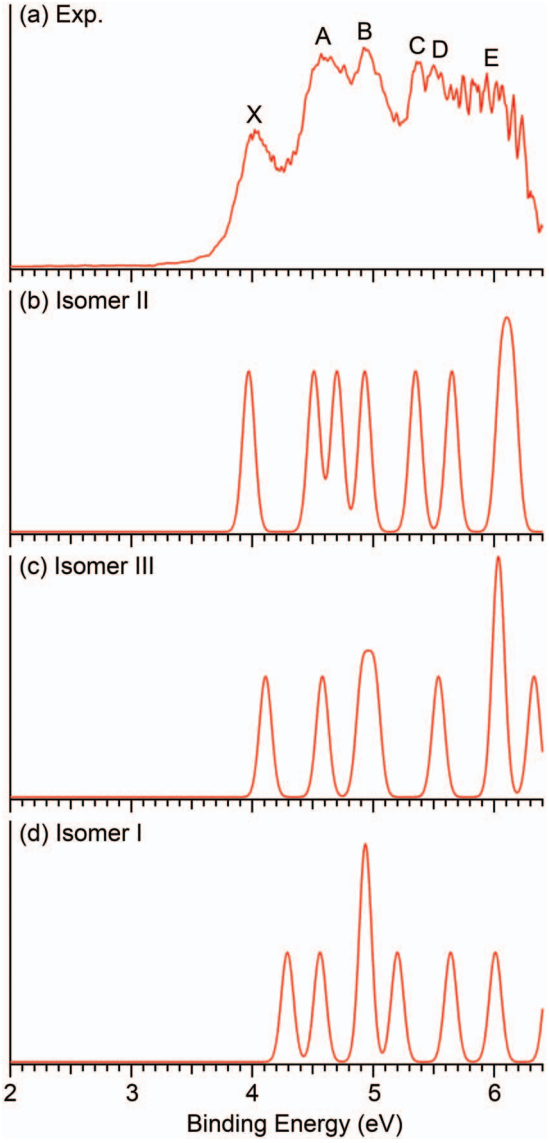

FIG. 4. Comparison between the simulated spectra for isomers **I, II,** and **III** with the experimental spectrum. The simulated spectra were created by fitting Gaussian functions with a 0.1 eV full width at half height to the TD-PBE0 VDE values.

identical VDEs for all other detachment channels. We also note that we could not calculate the VDEs with the ROVGF method for the two highest detachment channels given in Table I for isomer **II**. We should point out that the TD-DFT method, in general, has given excellent VDEs for relatively large boron clusters in our previous studies.[14–19]

B. Isomers I and III

The first VDE calculated for isomer **I** is 4.29 eV at TD-PBE0 (Table I), which lies between bands X and A. However, since bands X and A are not resolved to the baseline and there is substantial intensity in between, we could not rule out minor contributions from isomer **I**. The calculated VDEs from higher detachment channels of isomer **I** all overlap with the broad experimental spectrum (Table I and Fig. 4). We conclude that if it is present at all, isomer **I** would be expected to be weakly populated. A substantial presence of isomer **I** along with isomer **II** would likely yield a spectrum much less well resolved than that observed experimentally, on the basis of the sum of the predicted spectral patterns for the two isomers (Fig. 4).

The predicted first VDE for isomer **III**, 4.11 eV at TD-PBE0 and 3.89 eV at ROVGF (Table 4), also agrees well with the experimental VDE of the X band. The second VDE predicted for isomer **III** at TD-PBE0 agrees well with band A at 4.6 eV. The third and fourth detachment channels from isomer **III** have very similar VDEs, on the basis of TD-PBE0, and they are consistent with band B. However, band A is much broader than band B experimentally and they are in much better agreement with the predicted VDE pattern from isomer **II**, whereas the predicted VDE pattern for isomer **III** yield a much stronger or broader band B. Hence, if isomer **III** was present at all experimentally, it would also be expected to be weakly populated because any significant population of isomer **III** would produce a spectrum with a much stronger band B. Furthermore, the predicted VDE pattern for higher detachment channels beyond 5.2 eV from isomer **III** is also not in good agreement with the observed PES pattern, again suggesting that contributions from isomer **III** should be weak, if it was present experimentally.

In summary, the excellent agreement between the calculated VDEs for isomer **II** and the experimental PES spectral pattern lends considerable credence that it should the dominating isomer present experimentally and is likely the true global minimum of B_{25}^-, though contributions from isomers **I** and **III** cannot be ruled out and they could be weakly populated in the cluster beam.

VI. DISCUSSION

A. Chemical bonding analyses

The chemical bonding pictures of isomers **I**, **II**, and **III** are shown in Figs. 5–7 respectively, where results from AdNDP analyses for isomers **I** and **II** are given, whereas π orbitals are given for isomer **III** in comparison with those of a hydrocarbon (Fig. 7). Since these structures are not truly planar, σ- and π-bonding can only be approximately assigned; in the case of isomer **III** the π molecular orbitals shown in Fig. 7 are based on a flattened structure. The AdNDP method is an efficient tool to decipher the chemical bonding of 2D boron clusters because of the presence of both localized and delocalized bonding features. The appearance of pentagonal-pyramid-like units first observed in B_{24}^- was suggested to cause an increase of out-of-plane distortions due to the potential inclination of such clusters towards the formation of icosahedral units known in bulk structures of boron.[18] Interestingly, a similar central capped pentagonal boron moiety is found in the recently reported B_{18}^{2-} cluster,[22] in which the inner B_6 unit in B_{18}^{2-} is shown to undergo quasi-free rotation inside a B_{12} peripheral ring. It was found that the absence of any localized σ-bond between the inner ring and the peripheral boron atoms makes the system fluxional.[22] A pentagonal-pyramid-like unit is present in both isomers **I** and **II**, consistent with their relatively large out-of-plane

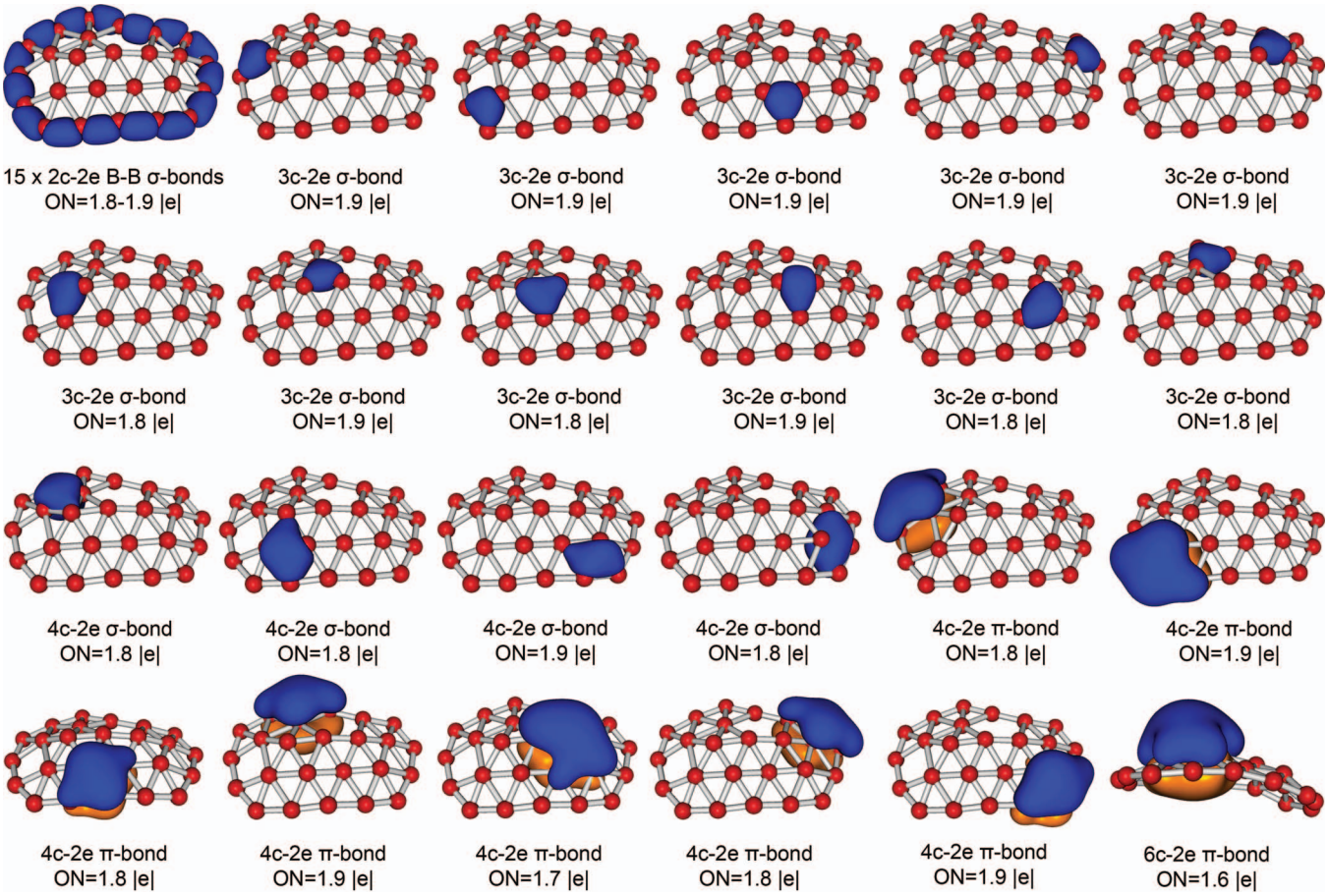

FIG. 5. AdNDP analyses for isomer **I** of B_{25}^-.

distortions. Similar to the bonding patterns observed in all smaller boron clusters investigated previously, classical 2c-2e B–B σ-bonds are found on the periphery for both isomers **I** and **II** with ON = 1.8−1.9 |e|, as shown in Figs. 5 and 6, respectively. Their peripheral B−B distances are very similar to each other: 1.53−1.67 Å for isomer **I** and 1.54−1.66 Å for isomer **II**. The same number of inner and outer atoms with approximately the same convex curvature of both isomers hints that their chemical bonding should be similar, as borne out by the AdNDP analyses. Figures 5 and 6 show that all the σ- and π-bonding elements display only slight deviations from each other. All of the σ-bonds associated with the ten inner atoms are found to be delocalized: eleven 3c-2e and four 4c-2e σ-bonds for isomer **I** and twelve 3c-2e and three 4c-2e σ-bonds for isomer **II**. There are three 3c-2e σ-bonds with ON = 1.8−1.9 |e| responsible for the bonding inside the pentagonal-pyramid-like unit in each isomer.

Besides the delocalized σ-bonds, ten inner boron atoms participate in the formation of eight delocalized π-bonds in both isomers: seven 4c-2e π-bonds and one 6c-2e π-bond in each case. It is noteworthy that the ONs of these bonds are slightly lower than the corresponding π bonds in the B_{21}^- and B_{24}^- clusters.[16,18] The lower ONs of the π bonds are a direct result of the increased out-of-plane distortion with increasing cluster size: from the almost planar B_{21}^- to a 1.2 Å deviation from the molecular plane in B_{24}^- and a 1.8 Å deviation from planarity in both isomers **I** and **II** of B_{25}^- (Fig. S2).[82] Isomer **I** contains five 4c-2e π-bonds around the pentagonal-pyramid-like unit. The other two 4c-2e π-bonds are found away from the pentagonal-pyramid-like unit and are responsible for bonding between three peripheral atoms and one interior atom. A unique chemical bonding element for isomer **I** is the 6c-2e π-bond, delocalized over the six atoms comprising the pentagonal-pyramid-like unit. A similar 6c-2e π-bond was also found in B_{19}^-, B_{21}^-, and B_{24}^- previously.[14,16,18] The increased out-of-plane distortion reduces the geometric stress imposed by the periphery in the larger clusters. The π-bonds found by the AdNDP analysis for isomer **II** look pretty similar to those of isomer **I**. Because one B–B bond on one side of the pentagonal-pyramid-like unit is longer in isomer **II**, an electron density rearrangement occurs, resulting in the shift of the 6c-2e π-bond to the edge of the cluster (Fig. 6).

The chemical bonding analysis of the ribbon-like isomer **III** was performed on the basis of the canonical molecular orbitals (CMOs). Since the C_{2v} structure is not perfectly planar, the division of the electron density into σ and π is done by flattening the structure (to D_{2h}) to prevent mixing of σ and π orbitals. The artificial flattening does not change the number of the CMOs and their nodal planes, and helps their visualization, because the out-of-plane distortions in isomer **III** are relatively small (~0.2 Å). We found eight π-CMOs reminiscent of those in dibenzopentalene ($C_{16}H_{10}$), which consists of two

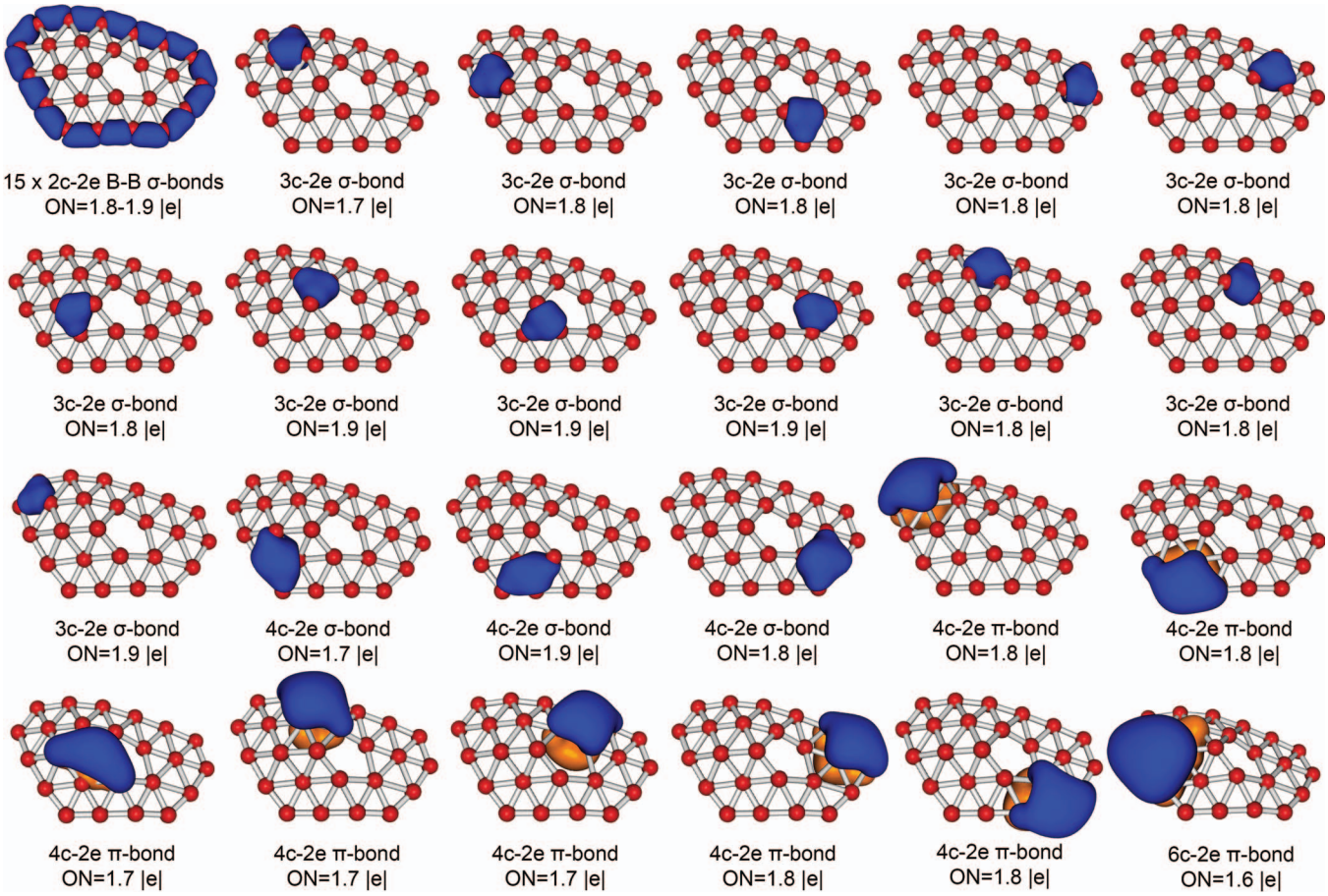

FIG. 6. AdNDP analyses for isomer **II** of B_{25}^-.

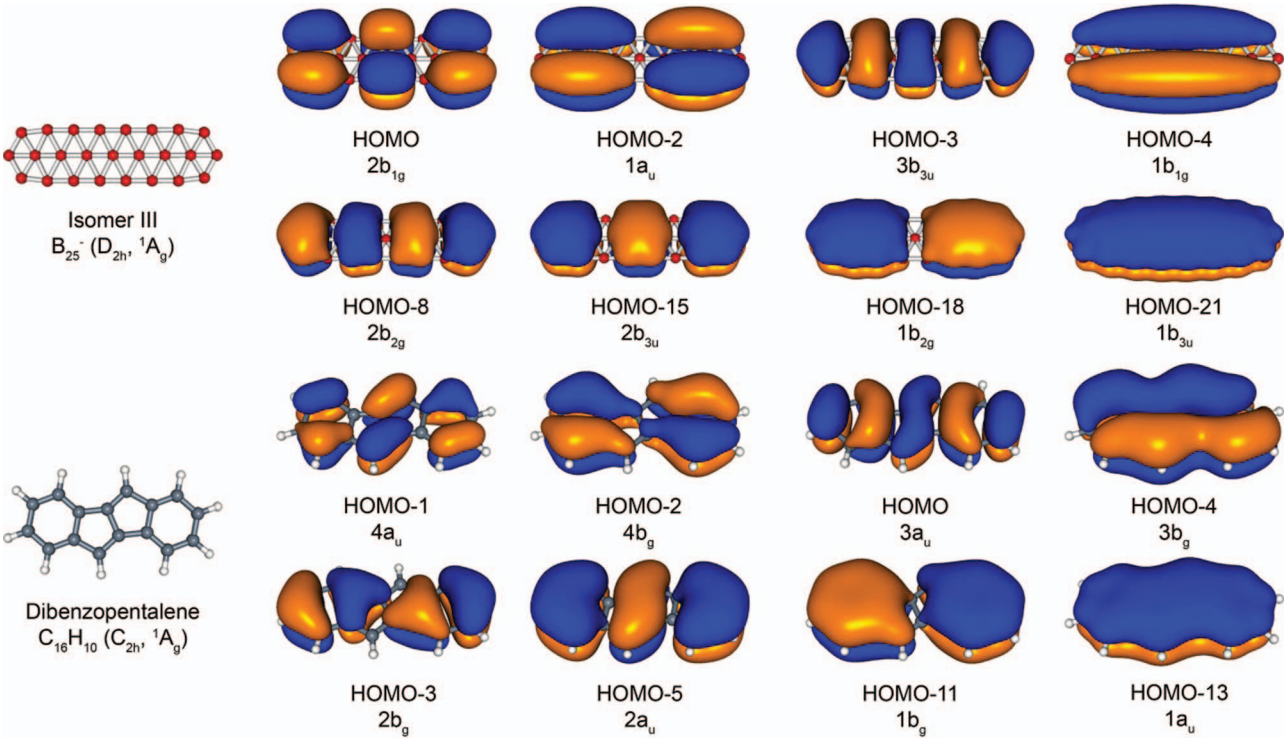

FIG. 7. Comparison of the π molecular orbitals of a flattened isomer **III** (D_{2h}) with those of dibenzopentalene $C_{16}H_{10}$.

benzene rings connected by the pentalene fragment (Fig. 7). The striking similarities between the π-CMOs of the boron cluster and the hydrocarbon show that the ribbon-like isomer **III** can be considered as an all-boron analogue of dibenzopentalene. Subsequent AdNDP analyses (not shown) revealed that the 18 peripheral boron atoms are described by classical 2c-2e σ-bonds (ON = 1.8−1.9|e|). The remaining electron density of isomer **III** is responsible for the bonding between the interior and the peripheral atoms in both delocalized σ- and π-bonds.

B. Structural evolution of anionic boron clusters

Isomers **I**, **II**, and **III** of B_{25}^- are all quasi-planar structures related to the familiar triangular grid motif of smaller boron clusters. Isomer **I** contains a pentagonal hole and a tetragonal hole, both near the edge of the structure, while isomer **II** contains only a pentagonal hole near the center of the cluster. Previous investigations[8–19] show that such defects are essential to keep the cluster flat, because of the unique chemical bonding in all 2D boron clusters, which exhibit strong peripheral B−B bonding and delocalized interior bonding. There seems to be a tendency for larger defect sizes from tetragonal → pentagonal → hexagonal holes as the cluster size increases. Figure 2 shows that the four nearest higher-lying isomers above isomer **III** all contain a hexagonal hole for B_{25}^-. As shown in Table S1 and mentioned in Sec. IV, a total of seven structures containing a hexagonal hole are found within 15 kcal/mol at the CCSD(T)/6-311+G(d) level of theory. The appearance of hexagonal holes in the low energy regions of the potential energy surface for B_{25}^- is noteworthy. The presence of low-lying isomers with hexagonal holes seems to be an ubiquitous feature of the potential energy surface for anionic boron clusters of $n > 20$. Our previous studies revealed four structures containing hexagonal holes within 20 kcal/mol of the global minimum for B_{21}^- and within 15 kcal/mol for B_{22}^- at the PBE0/6-311+G(d) level of theory.[16,17] The global minima and the low-lying structures exhibiting hexagonal holes for B_{21}^- and B_{22}^- are shown in Fig. S3.[82] Following the discovery of the hexagonally symmetric B_{36}^-, which has a central hexagonal hole,[49] the global minimum of B_{30}^- has been found very recently to be chiral, consisting of a pair of quasi-planar enantiomers both with a hexagonal hole.[50] One interesting question is at what size the first global minimum containing a hexagonal hole will be revealed for anionic boron clusters.

Isomer **III** represents a simple buckled triangular lattice in an elongated three-row ribbon form. In fact, this isomer can be viewed as extensions of the B_7^- cluster, which has a quasi-planar hexagonal global minimum,[10] by adding three boron atoms axially to form B_{10}^-,[9] B_{13}^-,[9] and B_{16}^-,[12] which all share the three-row ribbon motif and exist as definitive global minima. However, the next members of this series, B_{19}^- and B_{22}^-, do not have the ribbon-like structures as low-lying isomers.[14,17] Interestingly, double-row ribbon-like structures have been observed previously in boron dihydride and boron diboronyl clusters.[83,84]

VII. CONCLUSIONS

A joint photoelectron spectroscopic and theoretical study has been conducted to investigate the structures and chemical bonding of the B_{25}^- cluster. Extensive global minimum searches revealed three nearly degenerate quasi-planar structures (**I**, **II**, and **III**) with **I** being more stable than **II** and **III** by only 0.8 and 0.9 kcal/mol, respectively, at the CCSD(T) level of theory, while isomer **III** is predicted as the lowest in energy using DFT calculations (PBE0 and TPSSh). Isomers **I** and **II** both feature a 15-atom periphery with 10 interior atoms: isomer **I** contains both a tetragonal and a pentagonal hole near the edge of the cluster, whereas isomer **II** only contains an interior pentagonal hole. Isomer **III** is a nearly planar, ribbon-like three-row buckled structure with 7 internal and 18 peripheral atoms. Comparison with experiment reveals that isomer **II** is mainly responsible for the observed PES spectrum, while isomers **I** and **III** cannot be ruled out as contributors to the experiment. Chemical bonding analyses showed strong peripheral B−B bonding and delocalized σ and π interior bonding for all three isomers. Significant out-of-plane distortions are observed in isomers **I** and **II**, caused by the presence of a pentagonal-pyramid-like unit in the interior of each structure. Isomer **III** exhibits a π molecular orbital pattern analogous to the hydrocarbon dibenzopentalene $C_{16}H_{10}$ and can be considered as its all-boron analogue. Hence, the quasi-planar ribbon-like isomer extends the family of all-boron analogues of hydrocarbons. The potential energy surface of B_{25}^- is found to be quite complex with thirteen structures revealed within 10 kcal/mol. The high density of low-lying structural isomers and the fact that their relative ordering is dependent on the theoretical methods employed suggest that it is essential to compare theory with experiment in order to determine the global minima at this size range for boron clusters.

ACKNOWLEDGMENTS

We thank Dr. C. Romanescu for experimental assistance. The experimental work was supported by the National Science Foundation (NSF) (CHE-1263745 to L.S.W. and CHE-1057746 to A.I.B.). This work used the Extreme Science and Engineering Discover Environment (XSEDE), which was supported by the National Science Foundation (OCI-1053575) as well as resources at the Center for Computation and Visualization (CCV) at Brown University. Computing, data storage, and other resources from the Division of Research Computing in the Office of Research and Graduate Studies at Utah State University are gratefully acknowledged. I.A.P. would like to give special thanks to John Hanks at the Division of Research Computing in the Office of Research and Graduate Studies at Utah State University for making special accommodations, which allowed this research to be accomplished.

[1] X. Blase, A. Rubio, S. G. Louie, and M. L. Cohen, Europhys. Lett. **28**, 335 (1994).
[2] W. Q. Han, L. Wu, Y. Zhu, K. Watanabe, and T. Taniguchi, Appl. Phys. Lett. **93**, 223103 (2008).
[3] D. Golberg, Y. Bando, Y. Huang, T. Terao, M. Mitome, C. Tang, and C. Zhi, ACS Nano **4**, 2979 (2010).

[4]J. Dai, X. Wu, J. Yang, and X. C. Zeng, J. Phys. Chem. Lett. **5**, 393 (2014).
[5]H. J. Zhai, L. S. Wang, A. N. Alexandrova, and A. I. Boldyrev, J. Chem. Phys. **117**, 7917 (2002).
[6]H. J. Zhai, L. S. Wang, A. N. Alexandrova, and A. I. Boldyrev, J. Phys. Chem. A **107**, 9319 (2003).
[7]A. N. Alexandrova, A. I. Boldyrev, H.-J. Zhai, L.-S. Wang, E. Steiner, and P. W. Fowler, J. Phys. Chem. A **107**, 1359 (2003).
[8]H. J. Zhai, A. N. Alexandrova, K. A. Birch, A. I. Boldyrev, and L. S. Wang, Angew. Chem., Int. Ed. **42**, 6004 (2003).
[9]H. J. Zhai, B. Kiran, J. Li, and L. S. Wang, Nat. Mater. **2**, 827 (2003).
[10]A. N. Alexandrova, A. I. Boldyrev, H. J. Zhai, and L. S. Wang, J. Phys. Chem. A **108**, 3509 (2004).
[11]B. Kiran, S. Bulusu, H. J. Zhai, S. Yoo, X. C. Zeng, and L. S. Wang, Proc. Natl. Acad. Sci. U.S.A. **102**, 961 (2005); W. An, S. Bulusu, Y. Gao, and X. C. Zeng, J. Chem. Phys. **124**, 154310 (2006).
[12]A. P. Sergeeva, D. Y. Zubarev, H. J. Zhai, A. I. Boldyrev, and L. S. Wang, J. Am. Chem. Soc. **130**, 7244 (2008).
[13]L. L. Pan, J. Li, and L. S. Wang, J. Chem. Phys. **129**, 024302 (2008).
[14]W. Huang, A. P. Sergeeva, H. J. Zhai, B. B. Averkiev, L. S. Wang, and A. I. Boldyrev, Nat. Chem. **2**, 202 (2010).
[15]A. P. Sergeeva, B. B. Averkiev, H. J. Zhai, A. I. Boldyrev, and L. S. Wang, J. Chem. Phys. **134**, 224304 (2011).
[16]Z. A. Piazza, W. L. Li, C. Romanescu, A. P. Sergeeva, L. S. Wang, and A. I. Boldyrev, J. Chem. Phys. **136**, 104310 (2012).
[17]A. P. Sergeeva, Z. A. Piazza, C. Romanescu, W. L. Li, A. I. Boldyrev, and L. S. Wang, J. Am. Chem. Soc. **134**, 18065 (2012).
[18]I. A. Popov, Z. A. Piazza, W. L. Li, L. S. Wang, and A. I. Boldyrev, J. Chem. Phys. **139**, 144307 (2013).
[19]A. P. Sergeeva, I. A. Popov, Z. A. Piazza, W. L. Li, C. Romanescu, L. S. Wang, and A. I. Boldyrev, Acc. Chem. Res. **47**, 1349 (2014).
[20]J. O. C. Jiménez-Halla, R. Islas, T. Heine, and G. Merino, Angew. Chem., Int. Ed. **49**, 5668 (2010).
[21]T. B. Tai, A. Ceulemans, and M. T. Nguyen, Chem. Eur. J. **18**, 4510 (2012).
[22]D. Moreno, S. Pan, L. L. Zeonjuk, R. Islas, E. Osorio, G. Martinez-Guajardo, P. K. Chattaraj, T. Heine, and G. Merino, Chem. Commun. **50**, 8140 (2014).
[23]L. Hanley, J. L. Whitten, and S. L. Anderson, J. Phys. Chem. **92**, 5803 (1988).
[24]E. Oger, N. R. Crawford, R. Kelting, P. Weis, M. M. Kappes, and R. Ahlrichs, Angew. Chem., Int. Ed. **46**, 8503 (2007).
[25]G. Martínez-Guajardo, A. P. Sergeeva, A. I. Boldyrev, T. Heine, J. M. Ugalde, and G. Merino, Chem. Commun. **47**, 6242 (2011).
[26]J. Zhang, A. P. Sergeeva, M. Sparta, and A. N. Alexandrova, Angew. Chem., Int. Ed. **51**, 8512 (2012).
[27]G. Merino and T. Heine, Angew. Chem., Int. Ed. **51**, 10226 (2012).
[28]T. B. Tai, N. M. Tam, and M. T. Nguyen, Chem. Phys. Lett. **530**, 71 (2012).
[29]C. Romanescu, D. J. Harding, A. Fielicke, and L. S. Wang, J. Chem. Phys. **137**, 014317 (2012).
[30]N. Gonzalez Szwacki, A. Sadrzadeh, and B. Yakobson, Phys. Rev. Lett. **98**, 166804 (2007); **100**, 159901 (2008) (erratum).
[31]D. L. V. K. Prasad and E. D. Jemmis, Phys. Rev. Lett. **100**, 165504 (2008).
[32]J. Zhao, L. Wang, F. Li, and Z. Chen, J. Phys. Chem. A **114**, 9969 (2010).
[33]H. Li, N. Shao, B. Shang, L. F. Yuan, J. L. Yang, and X. C. Zeng, Chem. Commun. **46**, 3878 (2010).
[34]S. De, A. Willand, M. Amsler, P. Pochet, L. Genovese, and S. Goedecker, Phys. Rev. Lett. **106**, 225502 (2011).
[35]P. Pochet, L. Genovese, S. De, S. Goedecker, D. Caliste, S. A. Ghasemi, K. Bao, and T. Deutsch, Phys. Rev. B **83**, 081403(R) (2011).
[36]F. Li, P. Jin, D. E. Jiang, L. Wang, S. B. Zhang, J. Zhao, and Z. F. Chen, J. Chem. Phys. **136**, 074302 (2012).
[37]K. C. Lau and R. Pandey, J. Phys. Chem. C **111**, 2906 (2007).
[38]H. Tang and S. Ismail-Beigi, Phys. Rev. Lett. **99**, 115501 (2007).
[39]X. Yang, Y. Ding, and J. Ni, Phys. Rev. B **77**, 041402(R) (2008).
[40]K. C. Lau and R. Pandey, J. Phys. Chem. B **112**, 10217 (2008).
[41]Y. Ding, X. Yang, and J. Ni, Appl. Phys. Lett. **93**, 043107 (2008).
[42]H. Tang and S. Ismail-Beigi, Phys. Rev. B **80**, 134113 (2009).
[43]V. Bezugly, J. Kunstmann, B. Grundkotter-Stock, T. Frauenheim, T. Niehaus, and G. Cuniberti, ACS Nano **5**, 4997 (2011).
[44]T. R. Galeev, Q. Chen, J. C. Guo, H. Bai, C. Q. Miao, H. G. Lu, A. P. Sergeeva, S. D. Li, and A. I. Boldyrev, Phys. Chem. Chem. Phys. **13**, 11575 (2011); T. R. Galeev, B. D. Dunnington, J. R. Schmidt, and A. I. Boldyrev, Phys. Chem. Chem. Phys. **15**, 5022 (2013).
[45]X. Wu, J. Dai, Y. Zhao, Z. Zhuo, J. Yang, and X. C. Zeng, ACS Nano **6**, 7443 (2012).
[46]E. S. Penev, S. Bhowmick, A. Sadrzadeh, and B. I. Yakobson, Nano Lett. **12**, 2441 (2012).
[47]Y. Liu, E. S. Penev, and B. I. Yakobson, Angew. Chem., Int. Ed. **52**, 3156 (2013).
[48]H. Liu, J. Gao, and J. Zhao, Sci. Rep. **3**, 3238 (2013).
[49]Z. A. Piazza, H. S. Hu, W. L. Li, Y. F. Zhao, J. Li, and L. S. Wang, Nat. Commun. **5**, 3113 (2014).
[50]W. L. Li, Y. F. Zhao, H. S. Hu, J. Li, and L. S. Wang, Angew. Chem., Int. Ed. **53**, 5540 (2014).
[51]T. B. Tai, L. V. Duong, H. T. Pham, D. T. T. Maia, and M. T. Nguyen, Chem. Commun. **50**, 1558 (2014).
[52]D. J. Wales and J. P. K. Doye, J. Phys. Chem. A. **101**, 5111 (1997).
[53]L. S. Wang, H. S. Cheng, and J. Fan, J. Chem. Phys. **102**, 9480 (1995).
[54]J. Akola, M. Manninen, H. Häkkinen, U. Landman, X. Li, and L. S. Wang, Phys. Rev. B **60**, R11297(R) (1999).
[55]W. Huang and L. S. Wang, Phys. Rev. Lett. **102**, 153401 (2009).
[56]M. Saunders, J. Comput. Chem. **25**, 621 (2004).
[57]C. Adamo and V. Barone, J. Chem. Phys. **110**, 6158 (1999).
[58]J. P. Perdew, K. Burke, and M. Ernzerhof, Phys. Rev. Lett. **77**, 3865 (1996).
[59]B. Delley, J. Chem. Phys. **92**, 508 (1990).
[60]W. J. Pietro, M. M. Francl, W. J. Hehre, D. J. DeFrees, J. A. Pople, and J. S. Binkley, J. Am. Chem. Soc. **104**, 5039 (1982).
[61]J. Tao, J. Perdew, V. Staroverov, and G. Scuseria, Phys. Rev. Lett. **91**, 146401 (2003).
[62]M. S. Gordon, J. S. Binkley, J. A. Pople, W. J. Pietro, and W. J. Hehre, J. Am. Chem. Soc. **104**, 2797 (1982).
[63]T. Clark, J. Chandrasekhar, G. W. Spitznagel, and P. V. R. Schleyer, J. Comput. Chem. **4**, 294 (1983).
[64]J. Čížek, C. Moser, and R. LeFebvre, Adv. Chem. Phys. **14**, 35 (1969).
[65]G. D. Purvis, J. Chem. Phys. **76**, 1910 (1982).
[66]K. Raghavachari, G. W. Trucks, J. A. Pople, and M. Head-Gordon, Chem. Phys. Lett. **157**, 479 (1989).
[67]L. S. Cederbaum, J. Phys. B **8**, 290 (1975).
[68]J. V. Ortiz, Int. J. Quantum Chem., Chem. Symp. **36**, 321 (1989).
[69]J. S. Lin and J. V. Ortiz, Chem. Phys. Lett. **171**, 197 (1990).
[70]R. Bauernschmitt and R. Ahlrichs, Chem. Phys. Lett. **256**, 454 (1996).
[71]M. E. Casida, C. Jamorski, K. C. Casida, and D. R. Salahub, J. Chem. Phys. **108**, 4439 (1998).
[72]D. Y. Zubarev and A. I. Boldyrev, Phys. Chem. Chem. Phys. **10**, 5207 (2008).
[73]I. A. Popov and A. I. Boldyrev, Comput. Theor. Chem. **1004**, 5 (2013).
[74]I. A. Popov, V. F. Popov, K. V. Bozhenko, I. Cernusak, and A. I. Boldyrev, J. Chem. Phys. **139**, 114307 (2013).
[75]C. Romanescu, T. R. Galeev, W. L. Li, A. I. Boldyrev, and L. S. Wang, Acc. Chem. Res. **46**, 350 (2013).
[76]I. A. Popov, Y. Li, Z. Chen, and A. I. Boldyrev, Phys. Chem. Chem. Phys. **15**, 6842 (2013).
[77]I. A. Popov and A. I. Boldyrev, Eur. J. Org. Chem. **2012**, 3485 (2012).
[78]J. P. Foster and F. Weinhold, J. Am. Chem. Soc. **102**, 7211 (1980).
[79]A. E. Reed, L. A. Curtiss, and F. Weinhold, Chem. Rev. **88**, 899 (1988).
[80]M. J. Frisch, G. W. Trucks, H. B. Schlegel *et al.*, GAUSSIAN 09, Revision D.01, Gaussian, Inc., Wallingford, CT, 2004.
[81]U. Varetto, MOLEKEL 5.4.0.8, Swiss National Supercomputing Centre, Manno Switzerland, 2009.
[82]See supplementary material at http://dx.doi.org/10.1063/1.4879551 for the listing of the lowest 30 isomers, comparison of the structures between B_{25}^- and $B_{24}-$, low-lying isomers of B_{21}^- and B_{22}^-, calculated VDEs, simulated spectra, and the coordinates of the lowest isomers.
[83]W. L. Li, C. Romanescu, T. Jian, and L. S. Wang, J. Am. Chem. Soc. **134**, 13228 (2012).
[84]H. J. Zhai, Q. Chen, H. Bai, H. G. Lu, W. L. Li, S. D. Li, and L. S. Wang, J. Chem. Phys. **139**, 174301 (2013).